

Data Sketching and Stacking: A Confluence of Two Strategies for Predictive Inference in Gaussian Process Regressions with High-Dimensional predictors

Samuel Gailliot*, Rajarshi Guhaniyogi* and Roger D. Peng[†]

Abstract. The supplementary file contains additional simulation results.

MSC2020 subject classifications: Primary 00X00, 00X00; secondary 00X00.

Keywords: Bayesian predictive stacking, predictor sketching, Gaussian processes, high-dimensional predictors, manifold regression, posterior consistency.

1 Additional Simulation Results

To evaluate quality of predictive uncertainty, we calculate the coverage and length of 95% predictive intervals (PI) for SkGP and other competitors. This section presents coverage probability boxplots over 50 replications for $p = 10000$ in the swiss roll example and torus example in Figures 1 and 2, respectively. Figure 3 displays the median lengths of the 95% PI for all competitors for $p = 10000$ in both the swiss roll and torus examples. Results for predictive uncertainties for $p = 2000$ are presented in Section 3.3 of the main article.

Across all simulations, SkGP's 95% PI coverage is near the nominal level, with intervals widening as noise increases (higher τ^2). BART and SkBART show poor coverage with narrower PIs. RF and SkRF also exhibit undercoverage ($\sim 80\%$) with wider PIs than SkGP. In the swiss roll example, GP's coverage is similar to SkGP but with intervals about twice as wide. In the torus example, for $p = 10000$, SkGP produces narrower PIs than GP while maintaining similar coverage as noise increases. Overall, SkGP provides more precise and robust predictive uncertainty compared to its competitors.

arXiv: 2010.00000

*Department of Statistics, Texas A&M University, samuel.gailliot@stat.tamu.edu; [rajguhaniyogi@stat.tamu.edu](mailto:rjguhaniyogi@stat.tamu.edu)

[†]Department of Statistics and Data Sciences, University of Texas at Austin, roger.peng@austin.utexas.edu

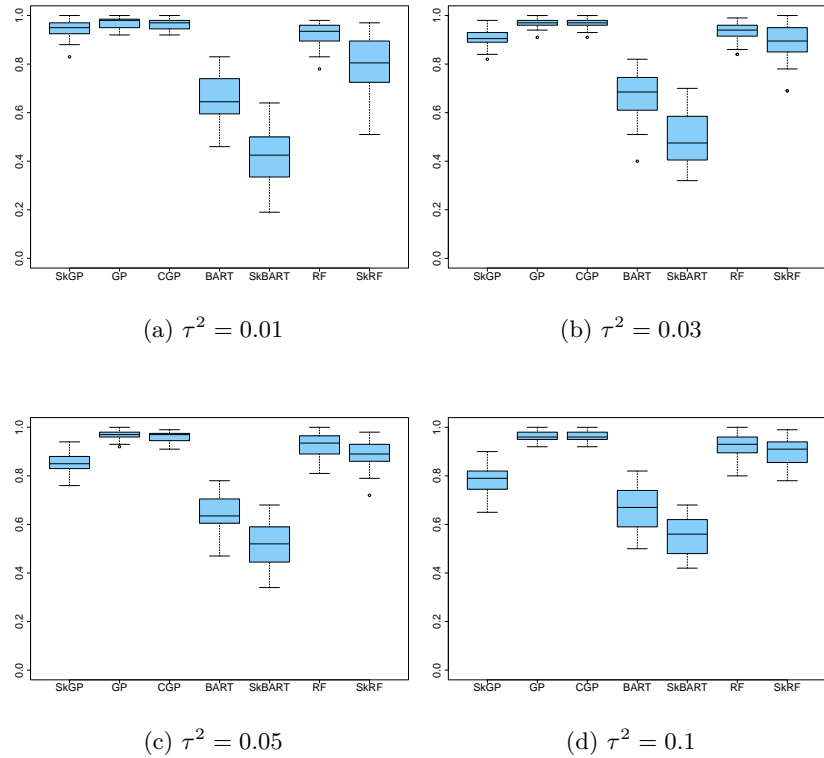


Figure 1: Coverage of 95% predictive interval for Swiss Roll Simulations for different noise levels τ^2 in the manifold containing predictors in the case of $p = 10000$.

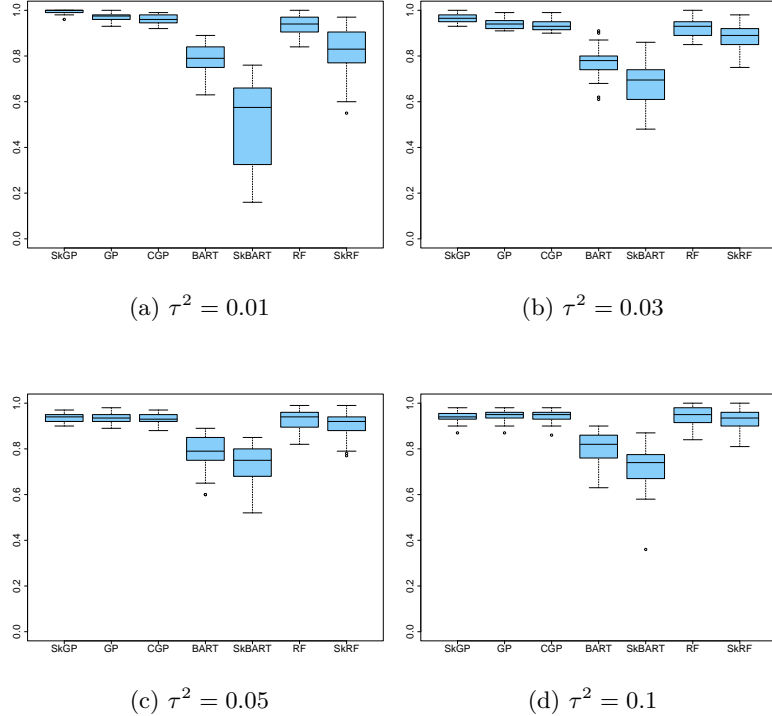


Figure 2: Coverage of 95% predictive interval for Torus Simulations for different noise levels τ^2 in the manifold containing predictors in the case of $p = 10000$.

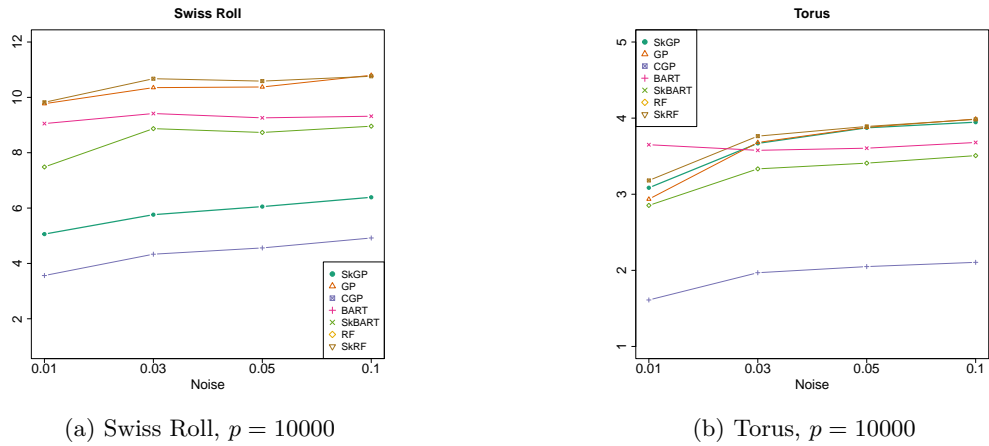


Figure 3: Length of 95% predictive intervals for all competitors in both swiss roll and torus simulations for $p = 10000$.

Data Sketching and Stacking: A Confluence of Two Strategies for Predictive Inference in Gaussian Process Regressions with High-Dimensional predictors

Samuel Gailliot*, Rajarshi Guhaniyogi** and Roger D. Peng[†]

Abstract. This article focuses on drawing computationally-efficient predictive inference from Gaussian process (GP) regressions with a large number of predictors when the response is conditionally independent of the predictors given the projection to a noisy low dimensional manifold. Bayesian estimation of the regression relationship using Markov Chain Monte Carlo and subsequent predictive inference is computationally prohibitive and may lead to inferential inaccuracies since accurate variable selection is essentially impossible in such high-dimensional GP regressions. As an alternative, this article proposes a strategy to sketch the high-dimensional predictor vector with a carefully constructed sketching matrix, before fitting a GP with the scalar outcome and the sketched predictor vector to draw predictive inference. The analysis is performed in parallel with many different sketching matrices and smoothing parameters in different processors, and the predictive inferences are combined using *Bayesian predictive stacking*. Since posterior predictive distribution in each processor is analytically tractable, the algorithm allows bypassing the robustness issues due to convergence and mixing of MCMC chains, leading to fast implementation with very large number of predictors. Simulation studies show superior performance of the proposed approach with a wide variety of competitors. The approach outperforms competitors in drawing point prediction with predictive uncertainties of outdoor air pollution from satellite images.

Keywords: Bayesian predictive stacking, predictor sketching, Gaussian processes, high-dimensional predictors, manifold regression, posterior consistency.

1 Introduction

We focus on the problem of drawing predictive inference of a random variable from a high-dimensional predictor vector using “sketching” of the predictor vector when it truly lies on a low-dimensional noisy unknown manifold. In recent years, there has been a growing literature on “data sketching,” which involves sketching or compressing the

*Rajarshi Guhaniyogi acknowledges funding from National Science Foundation through DMS-2220840 and DMS-2210672; and funding from National Institute of Health Award Number R01NS131604

[†]Department of Statistics, Texas A&M University, samuel.gailliot@stat.tamu.edu; rajguhaniyogi@stat.tamu.edu

[†]Department of Statistics and Data Sciences, University of Texas at Austin, roger.peng@austin.utexas.edu

original data before analysis [27, 38, 51, 22, 23]. However, our approach differs from the existing data sketching literature in two key aspects. Firstly, while most data sketching approaches aim to reduce the number of data samples, our approach is distinct in that it maintains the same number of samples but instead reduces the dimensionality of the predictor vector. Secondly, the majority of research in data sketching focuses on performance evaluation of ordinary and high-dimensional penalized regression methods with sketched data [57, 15, 17, 1, 29], with only a few recent articles considering application of data sketching in Bayesian high-dimensional linear and non-linear regressions [26, 22, 23]. In contrast, our approach demonstrates that when the predictor vector resides on a noisy unknown low-dimensional manifold, and the response has a nonlinear relationship with the predictors through the low-dimensional manifold coordinates, an exact nonparametric Bayesian framework can be employed—without the need for iterative sampling methods like Markov Chain Monte Carlo. This framework enables efficient and accurate predictions in ultra-high dimensions by effectively utilizing screening [20], data sketching, Gaussian process regression, and stacking of predictive distributions [55].

We consider a regression framework with an outcome $y \in \mathcal{Y} \subseteq \mathbb{R}$ and a predictor vector $\mathbf{x} = (x_1, \dots, x_p)^T$ when \mathbf{x} resides on a noisy unknown manifold, i.e., $\mathbf{x} = \phi(\mathbf{o}) + \boldsymbol{\eta}$, where $\mathbf{o} = (o_1, \dots, o_d)^T$ is d -dimensional co-ordinates for a manifold $\mathcal{O} \subseteq \mathbb{R}^p$, $\phi(\cdot) : \mathbb{R}^d \rightarrow \mathbb{R}^p$ is a mapping function such that $\phi(\mathbf{o}) \in \mathcal{O}$ and $\boldsymbol{\eta}$ is p -dimensional noise. Often the complex dependence between y and \mathbf{x} is encoded via co-ordinates of the low-dimensional manifold, i.e.,

$$y = h(\mathbf{o}) + \epsilon, \quad (1)$$

where h is a complex function encoding the true relationship between response and co-ordinates of the manifold and ϵ is the error. Since the manifold \mathcal{O} is unobserved, the co-ordinates \mathbf{o} is typically unknown. Hence, the common practice is to estimate complex dependencies between y and \mathbf{x} through a non-linear regression model given by,

$$y = f(\mathbf{x}) + \epsilon, \quad (2)$$

where f is an unknown regression function and ϵ is the residual. When dealing with high-dimensional predictors, Gaussian process (GP) priors with an automatic relevance determination (ARD) kernel are commonly used to estimate the underlying function f with sufficient sparsity assumption in the relationship between y and \mathbf{x} [58, 30]. The estimated f is then employed to predict the response variable. However, when the number of predictors reaches the order of a few thousand, estimation of f with GP-ARD framework is often inaccurate, leading to unsatisfactory predictive inference. This article proposes an alternative approach that exclusively focuses on drawing predictive inference on the response variable y , including both point prediction and uncertainty estimation, using GP regression. We review below a list of existing strategies to draw predictive inference on y in non-linear regressions before introducing our approach.

In the literature, a significant line of work follows a two-stage approach for dealing with high-dimensional predictors in non-linear manifold regression tasks. In this approach, the first stage involves constructing a lower-dimensional representation of the

high-dimensional predictors using manifold learning techniques. Some popularly employed parsimonious manifold learning algorithms include Isomap [44], Diffusion Maps [12], and Laplacian eigenmap [5]. These algorithms enable the reduction of dimensionality while preserving the essential characteristics of the data. Additionally, there are model-based approaches that estimate the unknown Riemannian manifold structure within the predictor vector. These methods utilize techniques such as local PCA [48, 3] or geometric multiresolution analysis [37], and, more recently, spherical basis functions [34]. Non-linear regression models in the second stage are based on these projected predictors in lower-dimensions. However, it is important to note that such two-stage approaches rely on learning the manifold structure embedded in the high-dimensional predictors. While this can be valuable for understanding the underlying data structure, it adds unnecessary computational burden when the primary focus is on prediction rather than inference.

An alternative line of research focuses on estimating the unknown function f using tree-based approaches or deep neural network methods. Tree-based approaches, such as CART [13], BART [11], and random forest [8] are based on finding the best splitting attribute, which can become less efficient as the number of predictors (p) increases. While there is a growing literature on variable selection within tree-based methods, such as BART [6] and its variants [36], estimating the true regression function with a large number of predictors (p of the order of thousands) can pose challenges. Deep neural networks with variable selection architecture [14] are also not ideal as they lack predictive uncertainty and struggle to handle the high-dimensional predictor space efficiently.

Bayesian modeling approaches are naturally appealing when the focus is on quantifying predictive uncertainty. To this end, the more traditional Bayesian models simultaneously learn the mapping to the lower-dimensional subspace along with the regression function in the coordinates on this subspace. These approaches range from Gaussian process latent variable models (GP-LVMs) [31, 46] for probabilistic nonlinear principle component analysis to mixture of factor models [9]. However, such methods pose daunting computational challenges with even moderately large p and sample size due to learning the number and distribution of latent variables, as well as the mapping functions, while maintaining identifiability restrictions.

To enhance the time efficiency of the aforementioned approaches, pre-processing steps are often employed, and two popular pre-processing methods are predictor screening and projection. The predictor screening approach identifies predictors that exhibit the strongest marginal association with the response variable. By selecting the predictors with the highest marginal association, this approach aims to reduce the dimensionality of the problem. predictor screening methods are generally straightforward to implement, and it offers asymptotic guarantees of selecting a superset of important predictors [10]. On the other hand, projection approaches aim to construct lower-dimensional predictor vectors by combining the original high-dimensional predictors. One common method in projection approaches is to construct a few principal components (PCs) from the original p -dimensional predictor vector.

A naive implementation of the above pre-processing steps is unappealing to our scenario. For example, in a non-parametric regression with a large number of correlated

predictors and low signal-to-noise ratio, it may be important to choose a conservative threshold for screening, which limits the scope of dimension reduction at this stage. On the other hand, construction of PCs are agnostic to the relationship between the response and the predictor vector. Instead, we propose an approach that first employs variable screening [10] with a conservative threshold to identify a large subset of predictors, typically a few thousand, having the highest non-linear marginal association with the response. After variable screening, the screened predictor vector is further compressed using a short and fat random sketching matrix [38, 16]. This matrix has a small number of rows (m) and entries that are independently and identically drawn from a normal distribution. Predictive inference proceeds by fitting a non-parametric Gaussian process (GP) regression model [49, 21] to the scalar outcome and the m -dimensional sketched predictor vector after fixing values for the weakly identifiable tuning parameters within the covariance kernel of the Gaussian processes. The posterior predictive distribution corresponding to a choice of such tuning parameters and random sketching matrix comes in a closed form without the need to implement MCMC sampling, so that one can obtain the predictive distribution extremely rapidly even in problems with huge numbers of predictors. To reduce the sensitivity of predictive inference to the choice of the sketching matrix and the tuning parameters in GP regression, the model is fit with multiple different choices of the sketching matrix and parameters. The predictive inferences obtained from such choices are then aggregated using Bayesian predictive stacking [55] to improve accuracy and robustness. When predictor vector lies on a low-dimensional unknown manifold and the response has a non-linear relationship with the manifold co-ordinates, the proposed approach has provable guarantee of drawing optimal predictive inference, as argued in this article.

Stacking is a model aggregation procedure to combine predictions from many different models [50, 7, 33]. In recent years, substantial advancements have been made in Bayesian stacking methodology, with notable contributions made in [32, 55, 41, 53, 54] and the references therein. However, the application of stacking in the context of predictive inference for high-dimensional manifold regression is currently lacking. While Bayesian model averaging [43] is most popularly used for aggregating inference from multiple models, it may be less suited to the stacking procedure in our settings. To see this, assume that there are S candidate models $\mathcal{M} = \{\mathcal{M}_1, \dots, \mathcal{M}_S\}$. Bayesian model comparison typically encounter three different settings: (i) \mathcal{M} -closed where a true data generating model exists and is included in \mathcal{M} ; (ii) \mathcal{M} -complete where a true model exists but is not included in \mathcal{M} ; and (iii) \mathcal{M} -open where we do not assume the existence of a true data generating model. Although Bayesian model averaging has the advantage of asymptotically identifying the true data generating model in the first setting, predictive stacking has advantages in the \mathcal{M} -complete and \mathcal{M} -open settings. Given that the true model may not be included in the class of fitted GP regression models with sketched predictors, predictive stacking offers substantial advantages over model averaging.

In regressions involving high-dimensional predictors and a large sample size, [26] propose an approach orthogonal to ours which exploits random sketching matrices to reduce the sample size rather than the number of predictors. A few approaches closely related to ours develop theoretical bound on predictive accuracy when high-dimensional predictors are sketched with random matrices [22, 23, 45]. These articles include random

linear combinations of many unimportant predictors, diminishing signal in the analysis, which results in less than satisfactory predictive performance with massive-dimensional predictors. Addressing this issue, [39] proposes novel constructions of projection matrices tailored to deliver more accurate predictive inference. These approaches aim to overcome the challenges associated with sketching high-dimensional predictors and improve predictive performance. However, they focus on high-dimensional parametric regression, and their applicability to non-parametric regression tasks may require further investigation. Moreover, these approaches address sensitivity to the choice of sketching matrices using Bayesian model averaging technique [43] which is less suitable for prediction than the stacking approach we employ here, as discussed in the last paragraph.

The rest of the article proceeds as follows. Section 1.1 discusses motivating dataset on outdoor air pollution and satellite imagery. Section 2 proposes the model and computational approach for predictive inference in manifold regression with large number of predictors. Section 3 offers empirical evaluation of the proposed approach along with its competitors for simulation studies. Section 4 investigates the proposed approach in drawing predictive inference of outdoor air pollution concentration from satellite images. Finally, Section 5 concludes the article with an eye towards future work.

1.1 Outdoor Air Pollution Application

As a motivation for the development of our methodology, we consider the problem of predicting outdoor air pollution concentrations across the United States. Outdoor air pollution in the U.S. is measured using a network of ground-based monitors managed by local air quality agencies and the U.S. Environmental Protection Agency [18] (EPA). While the combined network of monitors consists of thousands of locations, the spatial coverage of the network is actually quite sparse, leaving many areas of the country without any ground-level data [2]. To address the sparsity of the network, there have been efforts to deploy low-cost sensors across urban areas to fill the gaps. While such approaches have promise, they are still experimental and ad hoc in nature, and the sensors themselves can sometimes introduce new measurement problems [28].

Remote sensing techniques, which use satellite imagery to predict ground-level concentrations of outdoor air pollution have the potential to address the spatial coverage problem because of their constant monitoring of the entire planet. Traditional approaches have employed aerosol optical depth as a proxy for such pollutants as fine particulate matter [40], or PM2.5. In recent years, there has been a revolution in the deployment of satellite constellations, where hundreds of smaller inexpensive satellites orbit the Earth, providing constant coverage of all areas [42]. Furthermore, these satellites have much higher resolution. Given the recent emergence of data from satellite constellations, there is still a question of how best to use them for the purpose of predicting ground-level air pollution concentrations. For this application, we focus on predicting fine particulate matter pollution (PM2.5) from multi-band satellite images. For ground-truth information we use the EPA’s network of monitors to provide PM2.5 measurements. The combination of high-resolution spatial and temporal coverage of the entire U.S. with novel statistical predictive approaches has the potential to dramatically increase the monitoring of outdoor air pollution and its subsequent health effects.

2 Our Approach: Stacked Gaussian Process Regression

Let $\mathcal{D}_n = \{(\mathbf{x}_i^T, y_i) : i = 1, \dots, n\}$ be a dataset containing n observations each with a p -variate predictor $\mathbf{x}_i = (x_{i,1}, \dots, x_{i,p})^T$ and a scalar-valued response y_i . We assume n is moderately large and p is large. The predictor vector \mathbf{x}_i lies on an unknown noisy manifold $\mathcal{O} \subseteq \mathbb{R}^p$ with d -dimensional latent co-ordinates \mathbf{o}_i (i.e., $\mathbf{x}_i = \phi(\mathbf{o}_i) + \boldsymbol{\eta}_i$, $\phi(\mathbf{o}_i) \in \mathcal{O}$). We assume a nonlinear regression relationship between y_i and \mathbf{x}_i , and approximate the density of y_i by sketching the high-dimensional predictor vector \mathbf{x}_i to lower-dimensions using a sketching matrix \mathbf{P}_n as follows

$$y_i = f(\mathbf{P}_n \mathbf{x}_i) + \epsilon_i, \quad \epsilon_i \stackrel{i.i.d.}{\sim} N(0, \xi^2), \quad (3)$$

with ξ^2 as the noise variance and $f(\cdot)$ as an unknown continuous function in the Holder class of smoothness s . Discussion on the choice of the sketching matrix $\mathbf{P}_n \in \mathbb{R}^{m \times p}$ is provided in Section 2.1.

2.1 Choice of the Sketching Matrix

The sketching matrix $\mathbf{P}_n \in \mathbb{R}^{m \times p}$ embeds p -dimensional predictors \mathbf{x}_i into m dimensions while not throwing away excessive amounts of information. The most popular linear embedding is obtained from the singular value decomposition (SVD) of $\mathbf{X} = [\mathbf{x}_1 : \dots : \mathbf{x}_n]^T$, but they are problematic to estimate when $p \gg n$. In contrast, random sketching matrices are often used to embed the high-dimensional predictors to a random subspace, and appropriate choices of the random matrices allow distances between samples to be approximately preserved [35].

The direct application of sketching matrices on high-dimensional predictors is unappealing, as it constructs random linear combinations of many unimportant predictors, diminishing the signal in the analysis. As an alternative approach, we design a sketching matrix that constructs random linear combinations of predictors with the highest marginal association with the response. To identify these predictors, we perform nonparametric B-spline regression of y_i onto each component of \mathbf{x}_i separately. The order of importance of the predictors is determined, in descending order, by the residual sum of squares of the marginal nonparametric regressions. Predictors with a residual sum of squares greater than a user-defined threshold are considered important predictors related to the response. We adopt a conservative threshold following [20] to select a large superset of important predictors, which allows for joint contributions of predictors in explaining the response.

Let \mathcal{I} correspond to the indices of the predictors chosen with marginal screening and $\bar{\mathcal{I}}$ be the indices of the predictors screened out through this procedure, such that $\mathcal{I} \cup \bar{\mathcal{I}} = \{1, \dots, p\}$. Let \mathbf{E}_n be a permutation matrix such that $\mathbf{E}_n \mathbf{x} = (\mathbf{x}_{\mathcal{I}}^T, \mathbf{x}_{\bar{\mathcal{I}}}^T)^T$. We construct a matrix $\mathbf{R}_n = [\mathbf{R}_{n,1} : \mathbf{R}_{n,2}]$ where $\mathbf{R}_{n,2} = \mathbf{0}_{m \times (p - |\mathcal{I}|)}$ and $\mathbf{R}_{n,1}$ is an $m \times |\mathcal{I}|$ matrix with entries drawn independently from $N(0, 1)$, following the literature on random sketching matrices [4]. The resulting sketching matrix is given by $\mathbf{P}_n = \mathbf{R}_n \mathbf{E}_n$.

2.2 Prior, Posterior and Posterior Predictive Distributions

Following a Bayesian approach, we assign a zero-centered Gaussian process prior on the unknown regression function $f(\cdot)$, denoted by $f(\cdot) \sim GP(0, \sigma^2 \delta_\theta)$. Here, δ_θ corresponds to an exponential correlation kernel $\delta_\theta(\mathbf{x}_i, \mathbf{x}_j) = \exp(-\theta \|\mathbf{x}_i - \mathbf{x}_j\|)$ involving the length-scale parameter θ . The parameter σ^2 is the signal variance parameter and $\|\cdot\|$ denotes the Euclidean norm. A significant finding by [52] establishes that when predictors \mathbf{x}_i lie on a d -dimensional manifold \mathcal{O} , the minimax optimal rate of 1. The de-noised compressed predictors $\mathbf{P}_n \mathbf{x}_i$ exhibit a higher concentration around the manifold compared to the original predictors \mathbf{x}_i . With this enhanced concentration, the theory presented by [52] suggests that an appropriate GP prior can yield excellent performance. In addition to denoising, the compression of the high-dimensional predictor vector has a major advantage in avoiding the estimation of a geodesic distance along the unknown manifold \mathcal{O} between any two predictor vectors \mathbf{x}_i and $\mathbf{x}_{i'}$.

In practical applications, utilizing the recommended prior distributions on θ and σ^2 from [52] requires computationally expensive Markov Chain Monte Carlo (MCMC) sampling. In particular, the posterior computation of θ typically entails meticulous tuning, especially when dealing with high-dimensional predictors, imposing a significant computational burden. This article introduces an alternative approach that enables exact predictive inference from the model, entirely bypassing the MCMC algorithm in model estimation. The details of the strategy are elaborated below.

Denote $\mathbf{f} = (f(\mathbf{P}_n \mathbf{x}_1), \dots, f(\mathbf{P}_n \mathbf{x}_n))^T$ as the vector consisting of the function f evaluated at the sketched predictors $\mathbf{P}_n \mathbf{x}_1, \dots, \mathbf{P}_n \mathbf{x}_n$ and \mathbf{C} as an $n \times n$ covariance matrix with (i, j) th entry $\delta_\theta(\mathbf{P}_n \mathbf{x}_i, \mathbf{P}_n \mathbf{x}_j)$. With $\mathbf{y} = (y_1, \dots, y_n)^T$ as the response vector, a customary Bayesian hierarchical model is constructed as $\mathbf{y}|\mathbf{f}, \xi^2 \sim N(\mathbf{f}, \xi^2 \mathbf{I})$, $(\mathbf{f}|\xi^2) \sim N(0, \xi^2 \psi^2 \mathbf{C})$, $\pi(\xi^2) \propto \frac{1}{\xi^2}$, where we fix the length-scale parameter θ and the signal-to-noise variance ratio $\psi^2 = \frac{\sigma^2}{\xi^2}$. This ensures closed-form conjugate marginal posterior and posterior predictive distributions. More specifically, the marginal posterior distribution of ξ^2 , given the projection matrix \mathbf{P}_n , θ , ψ^2 and \mathcal{D}_n , is inverse gamma with parameters $a = n/2$ and $b = \mathbf{y}^T (\psi^2 \mathbf{C} + \mathbf{I})^{-1} \mathbf{y} / 2$. The marginal posterior distribution of \mathbf{f} , given \mathbf{P}_n , ψ^2 , θ and \mathcal{D}_n , follows a scaled n -variate t distribution with degrees of freedom n , location $\boldsymbol{\mu}_t$ and scale matrix $\boldsymbol{\Sigma}_t$, denoted by $t_n(\boldsymbol{\mu}_t, \boldsymbol{\Sigma}_t)$, where $\boldsymbol{\mu}_t = (\mathbf{I} + \mathbf{C}^{-1}/\psi^2)^{-1} \mathbf{y}$, $\boldsymbol{\Sigma}_t = (2b/n)(\mathbf{I} + \mathbf{C}^{-1}/\psi^2)^{-1}$. Consider prediction for the response at n_{new} data points with corresponding covariates $\tilde{\mathbf{x}}_1, \dots, \tilde{\mathbf{x}}_{n_{new}}$. Let $\mathbf{C}_{new,new}$ and $\mathbf{C}_{new,old}$ denote $n_{new} \times n_{new}$ and $n_{new} \times n$ matrices with (i, j) th elements $\delta_\theta(\mathbf{P}_n \tilde{\mathbf{x}}_i, \mathbf{P}_n \tilde{\mathbf{x}}_j)$ and $\delta_\theta(\mathbf{P}_n \tilde{\mathbf{x}}_i, \mathbf{P}_n \mathbf{x}_j)$, respectively. The posterior predictive distribution of the response $\tilde{\mathbf{y}}_{new} = (\tilde{y}_1, \dots, \tilde{y}_{n_{new}})^T$ given $\tilde{\mathbf{x}}_1, \dots, \tilde{\mathbf{x}}_{n_{new}}$, \mathbf{P}_n , θ , ψ^2 and \mathcal{D}_n , marginalizing out (\mathbf{f}, ξ^2) , follows a scaled n_{new} -variate t -distribution $t_{n_{new}}(\tilde{\boldsymbol{\mu}}_t, \tilde{\boldsymbol{\Sigma}}_t)$, where

$$\begin{aligned} \tilde{\boldsymbol{\mu}}_t &= \psi^2 \mathbf{C}_{new,old} (\mathbf{I} + \psi^2 \mathbf{C})^{-1} \mathbf{y} \\ \tilde{\boldsymbol{\Sigma}}_t &= (2b/n) [\mathbf{I} + \psi^2 \mathbf{C}_{new,new} - \psi^4 \mathbf{C}_{new,old} (\mathbf{I} + \psi^2 \mathbf{C})^{-1} \mathbf{C}_{new,old}^T]. \end{aligned} \quad (4)$$

Since the posterior predictive distribution is available in closed form, Bayesian inference can proceed from exact posterior samples.

This tractability is only possible if the length-scale parameter θ and the signal-to-noise variance ratio ψ^2 are fixed. While it is possible to estimate their full posterior distributions through expensive Markov Chain Monte Carlo (MCMC) sampling, these parameters are inconsistently estimable for the general Matern class of correlation functions [56] often resulting in poorer convergence. Therefore, for the chosen sketching matrix \mathbf{P}_n , we obtain (θ, ψ^2) such that

$$\max_{\theta, \psi^2} f(\theta, \psi^2 | \mathbf{P}_n, \mathbf{y}) \propto \max_{\theta, \psi^2} \frac{1}{|\psi^2 \mathbf{C} + \mathbf{I}|^{\frac{1}{2}}} \frac{2^{\frac{n}{2}} \Gamma(\frac{n}{2})}{[\mathbf{y}'(\psi^2 \mathbf{C} + \mathbf{I})^{-1} \mathbf{y}]^{\frac{n}{2}} (\sqrt{2\pi})^n} \quad (5)$$

Our approach will conduct exact predictive inference using the closed form predictive distribution in (4) and stack the predictive inference over different fixed values of $\{\mathbf{P}_n, \theta, \psi^2\}$.

Stacking of Predictive Distributions

Let \mathcal{M}_k represent the fitted model (3) with $\mathbf{P}_n^{(k)}, \theta^{(k)}, \psi^{2(k)}$ for $k = 1, \dots, K$. While the sketching matrix $\mathbf{P}_n^{(k)}$ is randomly generated for each k , $\theta^{(k)}$ and $\psi^{2(k)}$ are obtained following equation (5) for the choice of $\mathbf{P}_n^{(k)}$. Employing the generalized Bayesian stacking framework proposed by [55], we implement a stacking procedure over the predictive distribution obtained from each \mathcal{M}_k . Let $p(\tilde{\mathbf{y}}_{new} | \mathbf{y}, \mathcal{M}_k)$ denote the predictive distribution under model \mathcal{M}_k , and $p_t(\tilde{\mathbf{y}}_{new} | \mathbf{y})$ denote the true predictive distribution. Our objective is to determine the distribution in the convex hull $\mathcal{C} = \{\sum_{k=1}^K w_k p(\cdot | \mathbf{y}, \mathcal{M}_k) : w_k \in \mathcal{S}_1^K\}$, where $\mathcal{S}_1^K = \{\mathbf{w} \in [0, 1]^K : \sum_{k=1}^K w_k = 1\}$, that is optimal with respect to some proper scoring function. Using the logarithmic score, which corresponds to the KL divergence, we seek to find the vector $\tilde{\mathbf{w}} = (\tilde{w}_1, \dots, \tilde{w}_K)$ such that

$$\tilde{\mathbf{w}} = \max_{\mathbf{w} \in \mathcal{S}_1^K} \frac{1}{n} \sum_{i=1}^n \log \left(\sum_{k=1}^K w_k p_{k,-i}(y_i) \right), \quad (6)$$

where $\mathbf{y}_{-i} = (y_j : j \neq i, j = 1, \dots, n)^T$ and $p_{k,-i}(y_i) = p(y_i | \mathbf{y}_{-i}, \mathcal{M}_k)$ has a closed from univariate t -distribution with parameters $\tilde{\mu}_{-i}^{(k)}$ and $\tilde{\Sigma}_{-i}^{(k)}$ obtained using the formula for posterior predictive distribution given in equation (4). In practice, calculating the predictive densities $p_{k,-i}(y_i)$ one at a time is computationally expensive as the calculation of $\tilde{\Sigma}_{-i}^{(k)}$ requires inverting an $(n-1) \times (n-1)$ matrix for every $k = 1, \dots, K$ and $i = 1, \dots, n$. To avoid this, we randomly split the data into $S = 10$ disjoint folds of approximately equal size, $(\mathbf{y}_{(1)}, \mathbf{X}_{(1)}), \dots, (\mathbf{y}_{(S)}, \mathbf{X}_{(S)})$, and compute $\mathbf{y}_{(s)} | \mathbf{y}_{(1)}, \dots, \mathbf{y}_{(s-1)}, \mathbf{y}_{(s+1)}, \dots, \mathbf{y}_{(S)}$ for every $s = 1, \dots, S$, which follows a multivariate t -distribution with parameters obtained using equation (4). If the i th sample belongs to the s th fold, we will replace $p_{k,-i}(y_i)$ in (6) by $p_{k,(s)}(y_i)$, where $p_{k,(s)}(y_i)$ represents the marginal distribution of y_i from $\mathbf{y}_{(s)} | \mathbf{y}_{(1)}, \dots, \mathbf{y}_{(s-1)}, \mathbf{y}_{(s+1)}, \dots, \mathbf{y}_{(S)}$. This strategy requires inverting an $(n-n/S) \times (n-n/S)$ matrix only S times (assuming that all folds are of equal size), which leads to substantial computational benefits. No analytical solution to this non-convex constrained optimization problem in (6) is available, but first and second derivatives are easily obtained to construct an iterative optimizer.

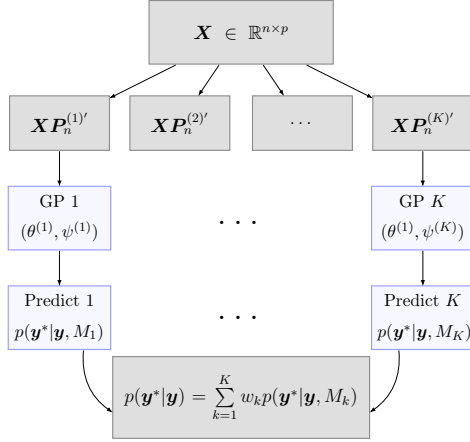


Figure 1: Flowchart representing the Sketched Gaussian process regression framework.

The optimal distribution provides a pseudo posterior predictive distribution given by $\tilde{p}(\tilde{\mathbf{y}}_{new}|\mathbf{y}) = \sum_{k=1}^K \tilde{w}_k t_{n_{new}}(\tilde{\boldsymbol{\mu}}_t^{(k)}, \tilde{\boldsymbol{\Sigma}}_t^{(k)})$, where $\tilde{\boldsymbol{\mu}}_t^{(k)}$ and $\tilde{\boldsymbol{\Sigma}}_t^{(k)}$ are obtained from equation (4) by evaluating $\tilde{\boldsymbol{\mu}}_t$ and $\tilde{\boldsymbol{\Sigma}}_t$ at $\mathbf{P}_n^{(k)}, \theta^{(k)}, \psi^{(k)}$. The pseudo posterior predictive distribution is further used to draw point prediction and 95% predictive interval to quantify predictive uncertainty. Figure 1 offers a flowchart outlining the proposed framework.

While Bayesian model averaging (BMA) is a common method for combining multiple distributions, its applicability in our context is limited for several reasons. Firstly, the fitted models (3) with randomly sketched predictors are likely to deviate from the true model, placing us outside the \mathcal{M} -closed setting where BMA is optimal. Additionally, stacking is designed to determine weights for optimal prediction, whereas asymptotically, BMA assigns full weight to the “best” single model closest in KL divergence to the true model [53]. However, when the true model lies outside the space of fitted models, it may be more advantageous to leverage multiple models in predictive inference. Subsequent empirical experiments demonstrate stacking as a powerful tool for drawing posterior predictive inference in our setting.

2.3 Theoretical Analysis

This section presents the theoretical foundation that explains the strong practical performance of the proposed method. In this context, when the predictor vector lies on a noisy manifold, i.e., $\mathbf{x} = \phi(\mathbf{o}) + \boldsymbol{\eta}$, it follows that $\mathbf{P}_n \mathbf{x} = \mathbf{P}_n \phi(\mathbf{o}) + \mathbf{P}_n \boldsymbol{\eta}$. Two key arguments support the claim that data sketching leads to nearly optimal inference:

- (A) When predictors lie exactly on a manifold, our proposed approach of GP regression with multiple sketched predictors followed by stacking achieves asymptoti-

cally accurate estimation of the true regression function. This shows that using the sketched predictors $\{\mathbf{P}_n\phi(\mathbf{o}_i)\}_{i=1}^n$ in our proposed approach will result in accurate asymptotic estimation of the regression function.

(B) Sketching the noise vector $\boldsymbol{\eta}$ with compression matrices reduces the impact of noise in \mathbf{x} on the overall performance.

To support (A), we first introduce the following definition and notations.

Definition: Let \mathcal{H}_1 and \mathcal{H}_2 be two manifolds. A differentiable map $g : \mathcal{H}_1 \rightarrow \mathcal{H}_2$ is called a diffeomorphism if it is a bijection and its inverse $g^{-1} : \mathcal{H}_2 \rightarrow \mathcal{H}_1$ is differentiable.

Let $f_k(\cdot)$ represent the fitted regression function for model \mathcal{M}_k , which corresponds to the fitted model (3) with parameters $\mathbf{P}_n^{(k)}, \theta^{(k)}, \psi^{2(k)}$ for $k = 1, \dots, K$. Let $f_0(\cdot)$ denote the true regression function. We define the distance between the stacked regression function and the true regression function under a fixed design of covariates lying on a manifold as $\Delta(f_0) = \frac{1}{n} \sum_{i=1}^n (\sum_{k=1}^K w_k f_k(\phi(\mathbf{o}_i)) - f_0(\phi(\mathbf{o}_i)))^2$. When the covariate design is random, this distance is expressed as $\Delta(f_0) = \int (\sum_{k=1}^K w_k f_k(\phi(\mathbf{o})) - f_0(\phi(\mathbf{o})))^2 dG$, where $G(\cdot)$ is the marginal distribution of the predictors. Let $\Pi(\cdot|\text{Data})$ represent the posterior distribution of the model parameters. The proposed method is said to be posterior consistent if $\Pi(\Delta(f_0) > \zeta|\text{Data}) \rightarrow 0$, as $n \rightarrow \infty$, for any $\zeta > 0$.

Lemma 2.1. Let $\Delta_k(f_0) = \frac{1}{n} \sum_{i=1}^n (f_k(\phi(\mathbf{o}_i)) - f_0(\phi(\mathbf{o}_i)))^2$ for fixed design and $\Delta_k(f_0) = \int (f_k(\phi(\mathbf{o})) - f_0(\phi(\mathbf{o})))^2 dG$ for random design of covariates. Assume that the stacking weights w_k , $1 \leq k \leq K$, are all bounded, then $\Pi(\Delta(f_0) > \zeta|\text{Data}) \rightarrow 0$, as $n \rightarrow \infty$, for any $\zeta > 0$.

Proof. For any $\zeta > 0$,

$$\begin{aligned} \Pi(\Delta(f_0) > \zeta|\text{Data}) &\leq \Pi\left(\sum_{k=1}^K \Delta_k(f_0) > \zeta / \sum_{k=1}^K w_k^2|\text{Data}\right) \\ &\leq \sum_{k=1}^K \Pi(\Delta_k(f_0) > \zeta / K \sum_{k=1}^K w_k^2|\text{Data}), \end{aligned} \quad (7)$$

where the second inequality follows by Cauchy-Schwartz theorem. Using Johnson-Lindenstrauss Lemma, the transformation $T(\phi(\mathbf{o}_i)) = \mathbf{P}_n\phi(\mathbf{o}_i)$ is a diffeomorphism onto its image with probability $\alpha_n \rightarrow 1$, as $n \rightarrow \infty$. If \mathcal{B}_n is the set where the function T is a diffeomorphism onto its image, we have $P(\mathcal{B}_n) = \alpha_n$. Hence,

$$\Pi(\Delta_k(f_0) > \zeta / K \sum_{k=1}^K w_k^2|\text{Data}) \leq \Pi(\Delta_k(f_0) > \zeta / K \sum_{k=1}^K w_k^2|\text{Data}, \mathcal{B}_n) P(\mathcal{B}_n) + P(\mathcal{B}_n^c). \quad (8)$$

$P(\mathcal{B}_n^c) = 1 - \alpha_n \rightarrow 0$, as $n \rightarrow \infty$. Considering all w_k 's are bounded and the function T is a diffeomorphism in \mathcal{B}_n , $\Pi(\Delta_k(f_0) > \zeta / K \sum_{k=1}^K w_k^2|\text{Data}, \mathcal{B}_n) \rightarrow 0$, as $n \rightarrow \infty$, following Theorem 2.3 of [52]. \square

Let $\mathbf{p}_{j,n}^{(k)}$ be the j th row of the matrix $\mathbf{P}_n^{(k)}$. According to Lemma 2.9.5 in [47], $\sqrt{|\mathcal{I}|}\mathbf{p}_{j,n}^{(k)}\boldsymbol{\eta} \rightarrow N(\mathbf{0}, \text{cov}(\phi(\mathbf{o}_1)))$. Therefore, it follows that $\mathbf{p}_{j,n}^{(k)}\boldsymbol{\eta} = O_p(|\mathcal{I}|^{-1/2})$. This demonstrates that the magnitude of the noise is reduced compared to the original predictors, thus proving (B). Consequently, the asymptotic performance of the proposed model using predictors $\{\mathbf{P}_n\mathbf{x}_i\}_{i=1}^n$ is nearly equivalent to the performance with $\{\mathbf{P}_n\phi(\mathbf{o}_i)\}_{i=1}^n$, thereby confirming the asymptotically accurate estimation of the true regression function, as established in (A).

3 Simulation Study

We evaluate the performance of Sketched Gaussian Process (SkGP) regression across various simulation scenarios, exploring different structure of the manifold (\mathcal{O}), predictor dimensions (p) and noise levels in the predictors (τ^2) to analyze their impact. In all simulations, the out-of-sample predictive performance of the proposed SkGP regression is compared with that of Gaussian Process (GP) with unsketched predictor vector which comes equipped with optimal prediction rate guarantees [52] when the predictor vector lies perfectly on a manifold, compressed GP (CompGP) where the unscreened features are sketched down to $m = 60$ once and predictions are made using a GP, Bayesian Additive Regression Trees (BART) [11], Random Forests (RF) [8], and deep neural network (NN). We also explore sketched versions of BART and RF, referred to as Sketched BART (SkBART) and Sketched Random Forest (SkRF), respectively, where a single projection matrix is generated to sketch the predictors, allowing for faster implementation. Each of these methods are applied on $|\mathcal{I}| = 1000$ screened predictors having highest marginal association with the response. As a default in this analysis, we set $m = 60$. We also introduce an additional competitor CompGP that first sketches a predictor vector to $|\mathcal{I}|$ dimensions and then screens the sketched predictors to m dimensions. We offer detailed sensitivity analysis with varying choices of the number of screened predictors $|\mathcal{I}|$ and the sketching dimensions m .

3.1 Simulated Data Generation

During data simulation, we explore specific scenarios where the response distribution follows a nonlinear function of d -dimensional coordinates for a manifold $\mathcal{O} \subseteq \mathbb{R}^p$, embedded in a high-dimensional ambient space. Two distinct choices for \mathcal{O} and their corresponding response distributions are simulated.

\mathcal{O} is a swiss roll and $d = 2$. For the swiss roll, we sample manifold coordinates, $\mathbf{o}_1 \sim U(\frac{3\pi}{2}, \frac{9\pi}{2})$, $\mathbf{o}_2 \sim U(0, 3)$. A high dimensional predictor $\mathbf{x} = (x_1, \dots, x_p)$ is simulated according to $x_1 = \mathbf{o}_1 \cos(\mathbf{o}_1) + \eta_1$, $x_2 = \mathbf{o}_2 + \eta_2$, $x_3 = \mathbf{o}_1 \sin(\mathbf{o}_1) + \eta_3$, $x_i = \eta_i$, $i \geq 4$. The response y have a non-linear relationship with these predictors and is simulated following,

$$y = \sin(5\pi\mathbf{o}_1) + \mathbf{o}_2^2 + \epsilon, \quad \epsilon \sim N(0, 0.02^2), \quad (9)$$

where $\eta_1, \dots, \eta_p \sim N(0, \tau^2)$. Notably, \mathbf{x} and y are conditionally independent given $\mathbf{o}_1, \mathbf{o}_2$ which is the low-dimensional signal manifold. In particular, \mathbf{x} lives on a (noise

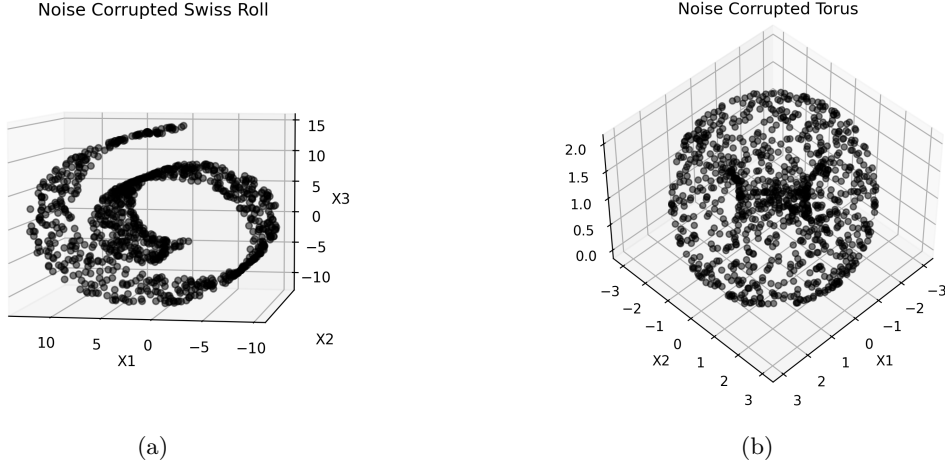


Figure 2: Manifolds embedded in noisy high-dimensional predictors.

corrupted) swiss roll embedded in a p -dimensional ambient space (see Figure 2a), but y is only a function of coordinates along the swiss roll \mathcal{O} .

\mathcal{O} is a torus and $d = 3$. For the torus, we consider $x_1 = o_1 + \eta_1, x_2 = o_2 + \eta_2$ and $x_3 = o_3 + \eta_3$ where o_1, o_2, o_3 lie on a three dimensional torus with interior radius 1 and exterior radius 3 (see Figure 2b), such that $(3 - \sqrt{o_1^2 + o_2^2})^2 + o_3^2 = 1$, and set $x_i = \eta_i$ for $i \geq 4$. The predictor noise η_1, \dots, η_n are generated i.i.d. from $N(0, \tau^2)$. The response is generated as,

$$y = o_2^2 + \sin(5\pi o_3) + \epsilon, \quad \epsilon \sim N(0, 0.1^2).$$

The geodesic distance between two points on both a swiss roll and a torus can substantially differ from their Euclidean distance in the ambient space \mathbb{R}^p . The swiss roll, in particular, poses a challenging setup for SkGP, as points on \mathcal{O} that are close in a Euclidean sense can be quite far in a geodesic sense.

To assess the impact of the number of predictors (p) and noise levels of the predictors (τ^2) on the performance of the competitors, various simulation scenarios are considered by varying $p = 2000, 10000$ and $\tau^2 = 0.01, 0.03, 0.05, 0.1$. For each of these simulation scenarios, 50 datasets are generated, and metrics such as mean squared prediction error (MSPE), coverage, and lengths of 95% predictive intervals (PI) are calculated across all replicates. All simulations set the sample size $n = 100$ and the number of predicted samples $n_{new} = 100$.

3.2 Point prediction

Tables 1 and 2 display the MSPE averaged over 50 replications for all the competing methods in the swiss roll and torus examples, respectively. Values in parentheses represent the standard error of MSPE over 50 replicates.

Both Tables 1 and 2 show that incorporating randomly sketched predictors into the GP model within the SkGP framework yields strong predictive performance, significantly surpassing the performance of the neural network. For both $p = 2000$ and $p = 10000$, when the manifold is affected by low noise, SkGP significantly outperforms GP, BART, and RF with unsketched predictors. While SkBART emerges as the second-best performer in scenarios with very low noise in the manifold ($\tau^2 = 0.01$), its performance declines notably with an increase in the noise level in the predictors. In comparison, SkGP effectively mitigates the impact of noise in the predictors, but there exists a tipping point (depending on the structure of the underlying manifold \mathcal{O} and sample size n) where noise distorts the manifold excessively, causing SkGP to perform similarly to other competitors. This is observed in the MSPE values corresponding to $\tau^2 = 0.1$. Among the sketched competitors, SkRF and CompGP exhibit notably inferior performance compared to both SkGP and SkBART in all simulation examples. While theoretically the performance of SkGP should remain similar for both $p = 2000$ and $p = 10000$ when all predictors lie exactly on a low-dimensional manifold, in practice, we observe a significant decline in the performance of SkGP with an increase in p . This is attributed to the substantial impact of noise corruption on the manifold, influencing predictive performance.

Swiss Roll		Noise			
		0.01	0.03	0.05	0.1
p = 2000	SkGP	0.96 (0.39)	1.27 (0.53)	1.74 (0.431)	3.26 (0.61)
	GP	1.28 (1.03)	1.75 (1.31)	2.49 (1.12)	4.81 (0.85)
	CompGP	5.9 (1.06)	6.84 (1.04)	7.13 (0.98)	7.41 (0.83)
	BART	2.31 (0.57)	2.28 (0.49)	2.35 (0.49)	2.57 (0.66)
	SkBART	0.91 (0.37)	1.62 (0.51)	2.63 (0.90)	5.17 (1.07)
	RF	6.92 (0.84)	6.87 (0.87)	6.92 (0.91)	6.97 (0.86)
	SkRF	0.99 (0.56)	2.05 (0.85)	3.28 (0.91)	5.84 (0.97)
	NN	3.52 (0.61)	6.66 (0.93)	7.41 (1.13)	8.47 (1.08)
p = 10,000	SkGP	1.64 (0.48)	2.55 (0.48)	3.57 (0.57)	4.54 (0.91)
	CompGP	5.84 (1.11)	5.84 (1.06)	7.25 (0.97)	7.33 (0.82)
	GP	5.19 (1.00)	5.65 (1.00)	6.16 (0.99)	7.08 (0.84)
	BART	4.17 (1.12)	4.07 (0.85)	4.33 (1.06)	4.37 (0.84)
	SkBART	2.38 (0.99)	5.33 (0.96)	6.34 (0.86)	7.31 (0.87)
	RF	7.32 (0.84)	7.30 (0.89)	7.32 (0.95)	7.35 (0.88)
	SkRF	3.57 (0.86)	5.72 (0.96)	6.66 (0.90)	7.46 (0.88)
	NN	7.32 (1.17)	8.88 (1.58)	10.15 (1.43)	10.80 (1.77)

Table 1: Averaged Mean squared Prediction Error (MSPE) over 50 replications are shown for the competing models in swiss roll example. Standard errors are presented within parenthesis.

3.3 Predictive Uncertainty

To evaluate quality of predictive uncertainty, we calculate the coverage and length of 95% predictive intervals (PI) for SkGP and competitors. While frequentist methods, like

Torus		Noise			
		0.01	0.03	0.05	0.1
p = 2000	SkGP	0.153 (0.036)	0.281 (0.072)	0.426 (0.108)	0.884 (0.127)
	GP	0.210 (0.081)	0.308 (0.085)	0.468 (0.104)	0.817 (0.119)
	CompGP	0.49 (0.15)	0.93 (0.14)	1 (0.13)	0.97 (0.13)
	BART	0.932 (0.132)	0.992 (0.137)	0.970 (0.137)	0.916 (0.152)
	SkBART	0.201 (0.084)	0.368 (0.092)	0.645 (0.151)	0.990 (0.139)
	RF	0.957 (0.132)	1.01 (0.124)	0.984 (0.124)	0.937 (0.132)
	SkRF	0.210 (0.091)	0.417 (0.103)	0.641 (0.132)	0.896 (0.127)
	NN	0.547 (0.139)	0.881 (0.122)	0.977 (0.086)	1.082 (0.130)
p = 10,000	SkGP	0.196 (0.048)	0.503 (0.103)	0.908 (0.121)	0.968 (0.136)
	CompGP	0.47 (0.13)	0.92 (0.14)	1 (0.13)	0.97 (0.13)
	GP	0.237 (0.077)	0.649 (0.110)	0.991 (0.129)	0.956 (0.132)
	BART	0.981 (0.129)	1.04 (0.128)	1.01 (0.129)	0.958 (0.132)
	SkBART	0.228 (0.096)	0.897 (0.152)	1.01 (0.130)	0.995 (0.136)
	RF	0.976 (0.136)	1.03 (0.128)	1.00 (0.125)	0.953 (0.129)
	SkRF	0.328 (0.102)	0.79 (0.139)	0.941 (0.131)	0.975 (0.131)
	NN	0.919 (0.114)	1.010 (0.117)	1.053 (0.125)	1.094 (0.118)

Table 2: Averaged Mean squared Prediction Error (MSPE) over 50 replications are shown for the competing models in torus example. Standard errors are presented within parenthesis.

SkRF and RF, do not inherently provide coverage probabilities with point estimates, we employ a two-stage plug-in approach for them: (i) estimate the regression function in the first stage, and (ii) construct 95% PI based on the normal distribution centered on the predictive mean from the regression model, with variance equal to the estimated variance in the residuals. Coverage probability boxplots over 50 replications for $p = 2000$ in the swiss roll example and torus example are presented in Figures 3 and 4, respectively. Figure 5 displays the median lengths of the 95% PI for all competitors for $p = 2000$ in both the swiss roll and torus examples. Results for predictive uncertainties for $p = 10000$ are presented in Section 1 of the supplementary file due to space constraint.

Across all simulations, SkGP's 95% PI coverage is near the nominal level, with intervals widening as noise increases (higher τ^2). BART and SkBART show poor coverage with narrower PIs. RF and SkRF also exhibit undercoverage ($\sim 80\%$) with wider PIs than SkGP. In the swiss roll example, GP's coverage is similar to SkGP but with intervals about twice as wide. In the torus example, GP and SkGP perform similarly for $p = 2000$, but for $p = 10000$, SkGP produces narrower PIs than GP while maintaining similar coverage as noise increases (see Section 1 of the supplementary file). Overall, SkGP provides more precise predictive uncertainty compared to its competitors.

3.4 Computation Time

The main goal of developing SkGP was to improve computational scalability in large p settings. For specific choices of \mathbf{P}_n , θ , and ψ^2 , the computation time is driven by

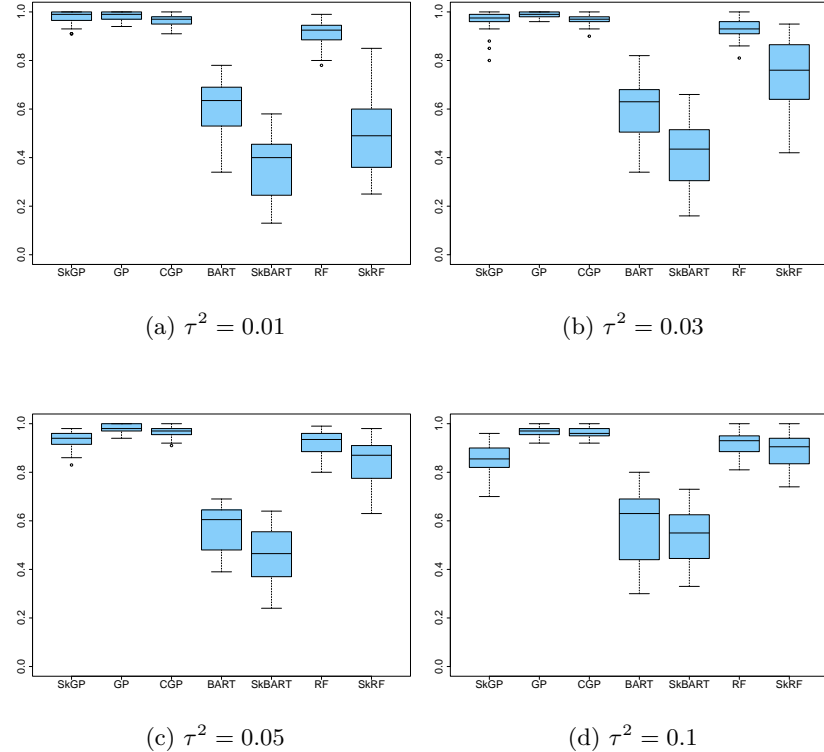


Figure 3: Coverage of 95% predictive interval for Swiss Roll Simulations for different noise levels τ^2 in the manifold containing predictors in the case of $p = 2000$.

two key factors: (a) inverting an $n \times n$ matrix, which has a complexity of n^3 , and (b) multiplying an $m \times |\mathcal{I}|$ matrix with an $|\mathcal{I}| \times n$ matrix, with a complexity of $mn|\mathcal{I}|$. Since the posterior predictive distribution is available in closed form, these computations are performed once per choice of \mathbf{P}_n , θ , and ψ^2 . Parallelization across different CPUs will handle various parameter choices efficiently. The stacking step involves inverting S matrices of dimension $(n - n/S) \times (n - n/S)$ with a complexity of $S(n - n/S)^3$. Given that the focus is on moderate n , all computations are highly efficient, enabling fast SkGP calculations.

Figure 6a demonstrates that as the number of predictors increases with a fixed sketching dimension ($m = 60$), computation times for non-sketched methods grow linearly, while sketched methods remain constant, depending only on the number of screened predictors $|\mathcal{I}|$. Figure 6b shows that as the sketching dimension increases with a fixed number of screened predictors ($|\mathcal{I}| = 1000$), computation times for sketched methods increase linearly. Importantly, SkGP achieves computation times comparable to frequentist approaches while enabling principled Bayesian predictive inference.

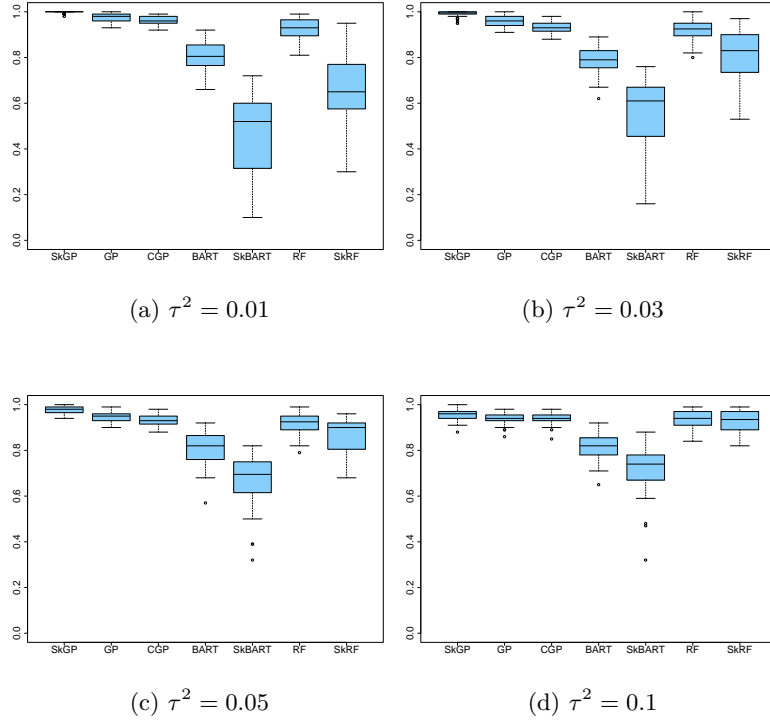


Figure 4: Coverage of 95% predictive interval for Torus Simulations for different noise levels τ^2 in the manifold containing predictors in the case of $p = 2000$.

3.5 Sensitivity to the choice of m , $|\mathcal{I}|$ and K

We investigate the impact of the number of predictors $|\mathcal{I}|$ selected based on their marginal association with the response and the sketching matrix dimension m applied to the $|\mathcal{I}|$ -dimensional predictor vector. Figure 7 shows MSPE values for the swiss roll example with varying numbers of included predictors $|\mathcal{I}|$. Due to the low intrinsic dimensionality of the swiss roll manifold and the response's dependence solely on the manifold, adding redundant predictors leads to performance degradation, as reflected by increasing MSPE, especially in high-noise settings. This confirms that estimating the regression function depends on the manifold's dimension, not the number of predictors.

Figure 8 illustrates the effect of sketching dimension m on SkGP performance. As m increases, MSPE decreases until reaching an optimal point, after which performance declines due to the introduction of redundant predictors. A sketching dimension of around $m \sim 50$ performs well across various examples with low-dimensional manifolds.

Figure 9 shows that increasing the number of models K reduces prediction variability, especially in high-noise scenarios. Stacking over many models increases the likelihood of sampling models with higher predictive accuracy.

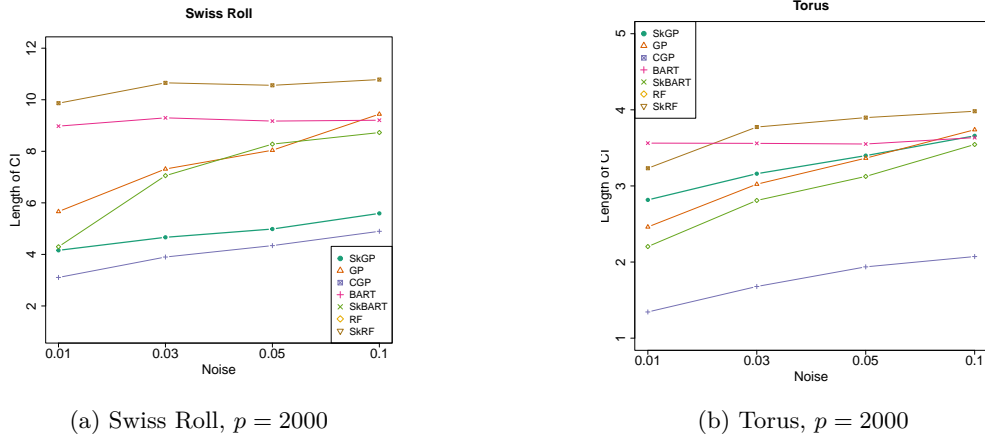


Figure 5: Length of 95% predictive intervals for all competitors in both swiss roll and torus simulations for $p = 2000$.

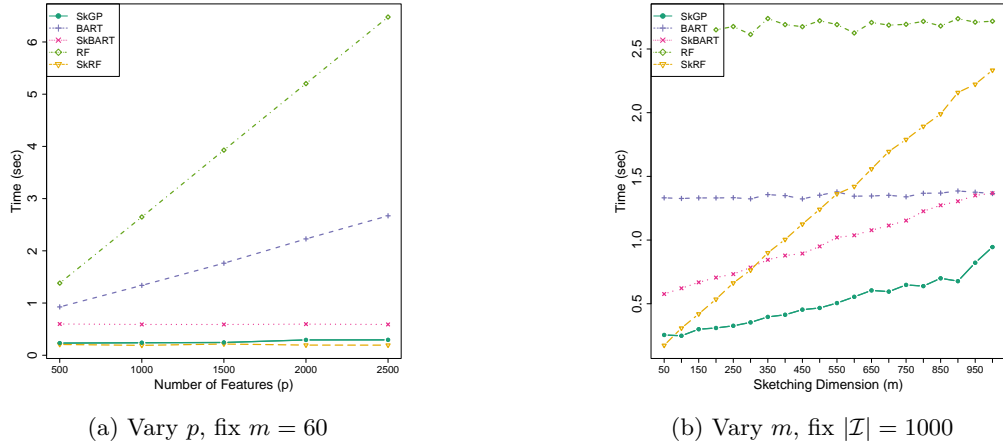


Figure 6: The left panel shows the computation time for competitors by fixing the sketching dimension (m), while varying the number of predictors. The right panel shows the computation time for competitors by fixing the number of screened predictors $|\mathcal{I}| = 1000$, while varying m .

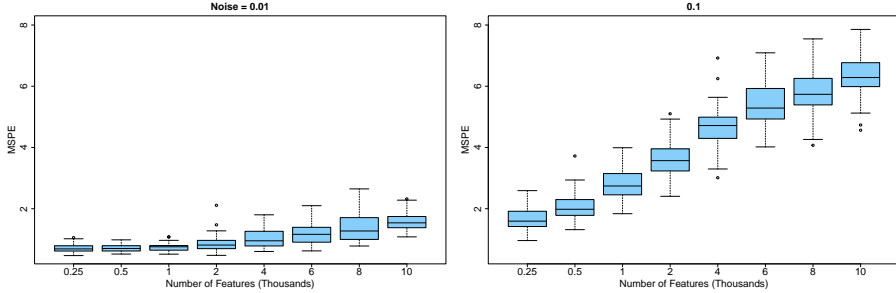


Figure 7: We show the number of included predictors \mathcal{I} through the nonparametric independent screening analysis vis-a-vis predictive accuracy. The left and right panels show plots corresponding to $\tau^2 = 0.01$ and $\tau^2 = 0.1$, respectively. The plots are presented for the swiss roll example.

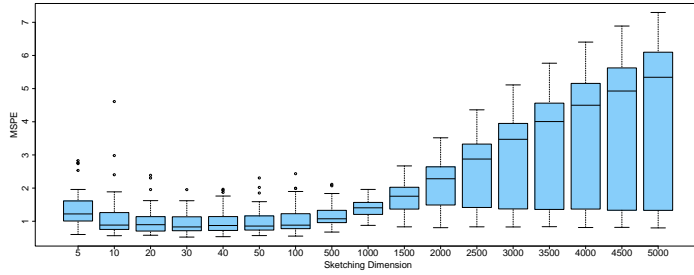


Figure 8: Plot of MSPE as sketching dimension (m) increases.

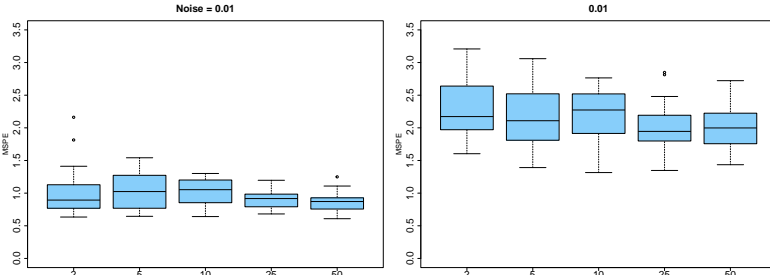


Figure 9: Left panel shows the plot of MSPE with changing number of models K to be stacked together with $\tau^2 = 0.01$. The right panel shows the same with $\tau^2 = 0.1$. Increasing the number of models (K) tends to increase predictive accuracy by decreasing the variation in predictions.

4 Analysis of Outdoor Air Pollution Data

We will apply the proposed approach and compare it with relevant competitors in the analysis of air quality using multi-band satellite images over time for 30 different cities in the USA. For each city, the dataset consists of almost daily air quality measurements from EPA federal reference monitors, sometimes with multiple readings in a day, collected between January 2019 and July 2022. We only consider data in this interval, since the data for dates prior to 2019 are sparse in many locations. This results in 1667 air quality measurements, as depicted in the first row of Figure 10. For each air quality reading, corresponding multi-band satellite images (blue, green, red, and near-infrared) were obtained from Planet’s PlanetScope instrument [42]. Since installing air quality monitors is costly, a key goal is to predict air quality using the high-dimensional multi-band images. At each time point, the $128 \times 128 = 16384$ pixels from the four bands are vectorized into a 65536-dimensional vector.

Although the images are high-dimensional, their intrinsic dimension (ID) determined using the two-nearest neighbor (NN) method [19] is much lower. For example, the estimated ID for Las Vegas is 4.18 with a standard error of 0.1, suggesting the vectorized image predictors lie on a lower-dimensional manifold, making it ideal for SkGP. Out of the 1667 samples, every fourth sample is used for testing, leaving $n = 1334$ training samples and $n_{new} = 333$ test samples.

The raw air quality monitor data in each city displays characteristics such as non-negativity, heavy-tailed distributions, non-stationary patterns, and periodic behavior. To meet the normality assumption for the error in (3), we apply a log transformation and standardize the response, ensuring a mean of zero and a variance of one. As an example, The first and the second row of Figure 10 illustrate the original and log-transformed and standardized air quality data for Las Vegas, respectively. Many of the pixels in the satellite images are zero at all times and are included to buffer the image to fit into a square. In our analysis, these zeros are removed. The columns of the image predictor matrix, with zeros removed, are pixel-wise standardized to have zero mean and unit variance. For each city, Nonparametric Independent Screening (NIS) [20] is used to identify predictors marginally related to air quality, retaining at least 5000 predictors to avoid discarding useful information.

Given that all other sketching approaches were inferior to SkGP, we focus our performance comparison with BART, considering BART as most competitive uncompressed method based on the simulation studies. Uncompressed GP is excluded due to its computational demands. Although the data has a temporal component, our current analysis does not account for time dynamics, which we plan to explore in future work.

In fitting SkGP, we use a sketching dimension of $m = 100$ and stack over $K = 20$ models. Table 3 shows that SkGP and BART perform similarly in point prediction across 30 cities. Although all competitors exhibit under-coverage, potentially due to neglecting the time-varying nature of the data, SkGP offers significantly better predictive uncertainty, achieving much higher coverage with slightly wider 95% predictive intervals. As an illustrative example, Figure 11 presents the predictive point estimates and 95% predictive interval bands across all hold-out time points in Las Vegas. Over-

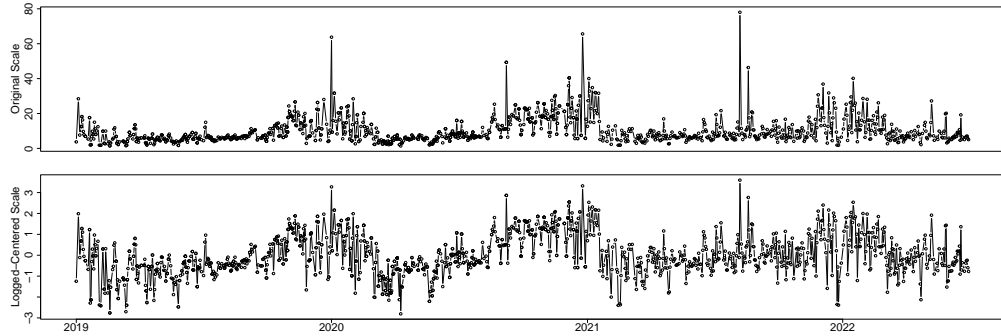


Figure 10: Daily air quality monitor data in Las Vegas. Original (top) and standardized for analysis (bottom). Data before 2019 contains irregular gaps and is excluded.

all, these findings highlight SkGP’s effectiveness in capturing the non-linear regression relationship between air quality and multi-band satellite images.

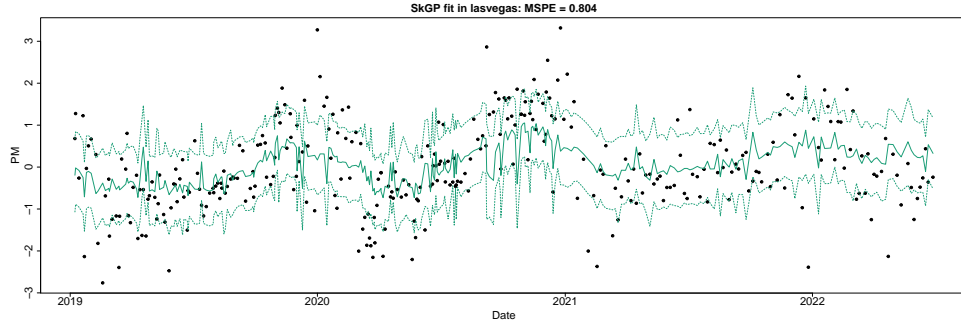


Figure 11: Point prediction and 95% predictive interval for Las Vegas PM2.5 test points. SkGP accurately recovers the trend with good coverage.

5 Conclusion and Future Work

This article is the first to present a novel Bayesian approach for predictive inference of outdoor air quality using high-resolution satellite images, when these images lie on a low-dimensional noise-corrupted manifold. Our methodology exploits two powerful ideas, data sketching and stacking, to eliminate the necessity for computationally demanding manifold structure estimation, providing accurate point predictions and predictive uncertainties. The computation of the posterior predictive distribution does not rely on MCMC sampling, and our framework is amenable to parallel implementation, resulting in substantial reductions in computation and storage costs. Empirical findings underscore the significantly improved point prediction and predictive uncertainty of our approach compared to existing methods.

Location	SkGP			BART		
	MSPE	Coverage	PI Length	MSPE	Coverage	PI Length
Akron	0.83	0.85	2.07	0.93	0.65	1.73
Albuquerque	0.87	0.93	2.10	0.83	0.67	1.59
Atlanta	0.96	0.79	2.27	1.01	0.51	1.51
Austin	0.89	0.86	2.23	0.95	0.65	1.78
Birmingham	0.88	0.78	2.132	0.93	0.52	1.37
Bismark	0.79	0.86	2.07	0.87	0.69	1.86
Boston	0.87	0.77	2.03	0.88	0.65	1.73
The Bronx	0.93	0.82	2.06	0.97	0.52	1.42
Broward	0.97	0.82	2.03	1.03	0.59	1.72
Cedar Rapids	0.85	0.81	2.04	0.93	0.63	1.82
Chattanooga	0.98	0.86	2.19	0.96	0.55	1.55
Chicago	0.98	0.84	2.29	1.02	0.56	1.67
Dallas	0.98	0.86	2.32	1.01	0.54	1.44
Fort Collins	0.64	0.90	1.85	0.66	0.69	1.61
Houston	0.90	0.88	2.30	0.93	0.62	1.70
Jackson	0.89	0.82	2.51	0.90	0.53	1.45
Las Vegas	0.80	0.80	1.89	0.92	0.59	1.40
Los Angeles	0.94	0.84	2.10	0.92	0.70	1.66
Merced	0.62	0.88	1.83	0.67	0.72	1.64
Phoenix	0.77	0.92	2.43	0.73	0.77	2.00
Pittsburgh	0.99	0.83	2.10	0.97	0.52	1.46
Queens	0.87	0.85	2.22	0.85	0.63	1.60
Raleigh	0.80	0.87	2.33	0.79	0.63	1.66
Salt Lake City	0.86	0.91	2.46	0.78	0.58	1.43
Saint Louis	0.96	0.95	3.12	0.92	0.48	1.39
Saint Paul	0.94	0.87	2.42	0.93	0.65	1.94
Terre Haute	1.11	0.89	1.86	1.10	0.61	1.56
Timonium	1.05	0.91	2.03	1.07	0.66	1.68
Tulsa	0.93	0.91	2.39	0.92	0.64	1.70
Yuma	0.84	0.91	2.41	0.92	0.66	1.69

Table 3: Results for 30 cities across the US. SkGP and BART yield comparable predictive accuracy. SkGP outperforms BART for uncertainty quantification in terms of coverage of 95% predictive intervals.

As an immediate future work, we will extend our framework to study joint predictive inference of outdoor air quality with remote-sensing images jointly over 30 cities. This investigation will naturally require the model to handle large p as well as large n . To handle large sample sizes we will explore distributed Bayesian inference [25, 24]. Additionally, exploring applications to non-Gaussian or multivariate outcomes, and simultaneous estimation of the intrinsic dimensionality of the manifold alongside predictive inference for the outcome are also part of our future research directions.

References

- [1] Ahfock, D., Astle, W. J., and Richardson, S. (2017). “Statistical properties of sketching algorithms.” *arXiv preprint arXiv:1706.03665*. [2](#)
- [2] Apte, J. S., Messier, K. P., Gani, S., Brauer, M., Kirchstetter, T. W., Lunden, M. M., Marshall, J. D., Portier, C. J., Vermeulen, R. C., and Hamburg, S. P. (2017). “High-resolution air pollution mapping with Google street view cars: exploiting big data.” *Environmental science & technology*, 51(12): 6999–7008. [5](#)
- [3] Arias-Castro, E., Lerman, G., and Zhang, T. (2017). “Spectral clustering based on local PCA.” *The Journal of Machine Learning Research*, 18(1): 253–309. [3](#)
- [4] Baraniuk, R., Davenport, M., DeVore, R., and Wakin, M. (2008). “A simple proof of the restricted isometry property for random matrices.” *Constructive approximation*, 28: 253–263. [6](#)
- [5] Belkin, M. and Niyogi, P. (2003). “Laplacian eigenmaps for dimensionality reduction and data representation.” *Neural computation*, 15(6): 1373–1396. [3](#)
- [6] Bleich, J., Kapelner, A., George, E. I., and Jensen, S. T. (2014). “Variable selection for BART: an application to gene regulation.” [3](#)
- [7] Breiman, L. (1996). “Stacked regressions.” *Machine learning*, 24: 49–64. [4](#)
- [8] — (2001). “Random forests.” *Machine learning*, 45: 5–32. [3](#), [11](#)
- [9] Chen, M., Silva, J., Paisley, J., Wang, C., Dunson, D., and Carin, L. (2010). “Compressive sensing on manifolds using a nonparametric mixture of factor analyzers: Algorithm and performance bounds.” *IEEE Transactions on Signal Processing*, 58(12): 6140–6155. [3](#)
- [10] Chen, Z., Fan, J., and Li, R. (2018). “Error variance estimation in ultrahigh-dimensional additive models.” *Journal of the American Statistical Association*, 113(521): 315–327. [3](#), [4](#)
- [11] Chipman, H. A., George, E. I., and McCulloch, R. E. (2010). “BART: Bayesian additive regression trees.” [3](#), [11](#)
- [12] Coifman, R. R. and Lafon, S. (2006). “Diffusion maps.” *Applied and computational harmonic analysis*, 21(1): 5–30. [3](#)
- [13] Denison, D. G., Mallick, B. K., and Smith, A. F. (1998). “A bayesian cart algorithm.” *Biometrika*, 85(2): 363–377. [3](#)
- [14] Dinh, V. C. and Ho, L. S. (2020). “Consistent feature selection for analytic deep neural networks.” *Advances in Neural Information Processing Systems*, 33: 2420–2431. [3](#)
- [15] Dobriban, E. and Liu, S. (2018). “A new theory for sketching in linear regression.” *arXiv preprint arXiv:1810.06089*. [2](#)
- [16] Drineas, P., Magdon-Ismail, M., Mahoney, M. W., and Woodruff, D. P. (2012).

“Fast approximation of matrix coherence and statistical leverage.” *The Journal of Machine Learning Research*, 13(1): 3475–3506. 4

[17] Drineas, P., Mahoney, M. W., Muthukrishnan, S., and Sarlós, T. (2011). “Faster least squares approximation.” *Numerische mathematik*, 117(2): 219–249. 2

[18] Environmental Protection Agency (1996). *Air Quality Criteria for Particulate Matter*. EPA/600/P-95/001aF. Office of Research and Development, Washington DC. 5

[19] Facco, E., d’Errico, M., Rodriguez, A., and Laio, A. (2017). “Estimating the intrinsic dimension of datasets by a minimal neighborhood information.” *Scientific reports*, 7(1): 12140. 19

[20] Fan, J., Ma, Y., and Dai, W. (2014). “Nonparametric independence screening in sparse ultra-high-dimensional varying coefficient models.” *Journal of the American Statistical Association*, 109(507): 1270–1284. 2, 6, 19

[21] Gramacy, R. B. (2020). *Surrogates: Gaussian process modeling, design, and optimization for the applied sciences*. CRC press. 4

[22] Guhaniyogi, R. and Dunson, D. B. (2015). “Bayesian compressed regression.” *Journal of the American Statistical Association*, 110(512): 1500–1514. 2, 4

[23] — (2016). “Compressed Gaussian process for manifold regression.” *The Journal of Machine Learning Research*, 17(1): 2472–2497. 2, 4

[24] Guhaniyogi, R., Li, C., Savitsky, T., and Srivastava, S. (2023). “Distributed Bayesian inference in massive spatial data.” *Statistical science*, 38(2): 262–284. 21

[25] Guhaniyogi, R., Li, C., Savitsky, T. D., and Srivastava, S. (2022). “Distributed Bayesian varying coefficient modeling using a Gaussian process prior.” *The Journal of Machine Learning Research*, 23(1): 3642–3700. 21

[26] Guhaniyogi, R. and Scheffler, A. (2021). “Sketching in Bayesian High Dimensional Regression With Big Data Using Gaussian Scale Mixture Priors.” *arXiv preprint arXiv:2105.04795*. 2, 4

[27] Halko, N., Martinsson, P.-G., and Tropp, J. A. (2011). “Finding structure with randomness: Probabilistic algorithms for constructing approximate matrix decompositions.” *SIAM review*, 53(2): 217–288. 2

[28] Heffernan, C., Peng, R., Gentner, D. R., Koehler, K., and Datta, A. (2023). “A dynamic spatial filtering approach to mitigate underestimation bias in field calibrated low-cost sensor air pollution data.” *The Annals of Applied Statistics*, 17(4): 3056–3087. 5

[29] Huang, Z. (2018). “Near optimal frequent directions for sketching dense and sparse matrices.” In *International Conference on Machine Learning*, 2048–2057. PMLR. 2

[30] Jensen, K., Kao, T.-C., Stone, J., and Hennequin, G. (2021). “Scalable Bayesian

GPFA with automatic relevance determination and discrete noise models.” *Advances in Neural Information Processing Systems*, 34: 10613–10626. [2](#)

[31] Lawrence, N. and Hyvärinen, A. (2005). “Probabilistic non-linear principal component analysis with Gaussian process latent variable models.” *Journal of machine learning research*, 6(11). [3](#)

[32] Le, T. and Clarke, B. (2017). “A Bayes interpretation of stacking for M-complete and M-open settings.” [4](#)

[33] LeBlanc, M. and Tibshirani, R. (1996). “Combining estimates in regression and classification.” *Journal of the American Statistical Association*, 91(436): 1641–1650. [4](#)

[34] Li, D., Mukhopadhyay, M., and Dunson, D. B. (2022). “Efficient manifold approximation with spherelets.” *Journal of the Royal Statistical Society Series B: Statistical Methodology*, 84(4): 1129–1149. [3](#)

[35] Li, G. and Gu, Y. (2017). “Restricted isometry property of gaussian random projection for finite set of subspaces.” *IEEE Transactions on Signal Processing*, 66(7): 1705–1720. [6](#)

[36] Liu, Y., Rockova, V., and Wang, Y. (2021). “Variable selection with ABC Bayesian forests.” *Journal of the Royal Statistical Society Series B: Statistical Methodology*, 83(3): 453–481. [3](#)

[37] Maggioni, M., Minsker, S., and Strawn, N. (2016). “Multiscale dictionary learning: non-asymptotic bounds and robustness.” *The Journal of Machine Learning Research*, 17(1): 43–93. [3](#)

[38] Mahoney, M. W. et al. (2011). “Randomized algorithms for matrices and data.” *Foundations and Trends® in Machine Learning*, 3(2): 123–224. [2](#), [4](#)

[39] Mukhopadhyay, M. and Dunson, D. B. (2020). “Targeted random projection for prediction from high-dimensional features.” *Journal of the American Statistical Association*, 115(532): 1998–2010. [5](#)

[40] Paciorek, C. J., Liu, Y., Moreno-Macias, H., and Kondragunta, S. (2008). “Spatiotemporal associations between GOES aerosol optical depth retrievals and ground-level PM2. 5.” *Environmental science & technology*, 42(15): 5800–5806. [5](#)

[41] Pavlyshenko, B. M. (2020). “Using bayesian regression for stacking time series predictive models.” In *2020 IEEE Third International Conference on Data Stream Mining & Processing (DSMP)*, 305–309. IEEE. [4](#)

[42] Planet Team (2017). “Planet application program interface: In space for life on Earth.” *San Francisco, CA*, 2017(40): 2.
URL <https://www.planet.com> [5](#), [19](#)

[43] Raftery, A. E., Madigan, D., and Hoeting, J. A. (1997). “Bayesian model averaging for linear regression models.” *Journal of the American Statistical Association*, 92(437): 179–191. [4](#), [5](#)

[44] Tenenbaum, J. B., Silva, V. d., and Langford, J. C. (2000). “A global geometric framework for nonlinear dimensionality reduction.” *science*, 290(5500): 2319–2323. [3](#)

[45] Thanei, G.-A., Heinze, C., and Meinshausen, N. (2017). “Random projections for large-scale regression.” *Big and Complex Data Analysis: Methodologies and Applications*, 51–68. [4](#)

[46] Titsias, M. and Lawrence, N. D. (2010). “Bayesian Gaussian process latent variable model.” In *Proceedings of the thirteenth international conference on artificial intelligence and statistics*, 844–851. JMLR Workshop and Conference Proceedings. [3](#)

[47] Van Der Vaart, A. W., Wellner, J. A., van der Vaart, A. W., and Wellner, J. A. (1996). *Weak convergence*. Springer. [11](#)

[48] Weingessel, A. and Hornik, K. (2000). “Local PCA algorithms.” *IEEE Transactions on neural Networks*, 11(6): 1242–1250. [3](#)

[49] Williams, C. K. and Rasmussen, C. E. (2006). *Gaussian processes for machine learning*, volume 2. MIT press Cambridge, MA. [4](#)

[50] Wolpert, D. H. (1992). “Stacked generalization.” *Neural networks*, 5(2): 241–259. [4](#)

[51] Woodruff, D. P. et al. (2014). “Sketching as a tool for numerical linear algebra.” *Foundations and Trends® in Theoretical Computer Science*, 10(1–2): 1–157. [2](#)

[52] Yang, Y. and Dunson, D. B. (2016). “Bayesian manifold regression.” [7](#), [10](#), [11](#)

[53] Yao, Y., Pirs, G., Vehtari, A., and Gelman, A. (2022). “Bayesian hierarchical stacking: Some models are (somewhere) useful.” *Bayesian Analysis*, 17(4): 1043–1071. [4](#), [9](#)

[54] Yao, Y., Vehtari, A., and Gelman, A. (2022). “Stacking for non-mixing Bayesian computations: The curse and blessing of multimodal posteriors.” *The Journal of Machine Learning Research*, 23(1): 3426–3471. [4](#)

[55] Yao, Y., Vehtari, A., Simpson, D., and Gelman, A. (2018). “Using stacking to average Bayesian predictive distributions (with discussion).” [2](#), [4](#), [8](#)

[56] Zhang, H. (2004). “Inconsistent estimation and asymptotically equal interpolations in model-based geostatistics.” *Journal of the American Statistical Association*, 99(465): 250–261. [8](#)

[57] Zhang, L., Mahdavi, M., Jin, R., Yang, T., and Zhu, S. (2013). “Recovering the optimal solution by dual random projection.” In *Conference on Learning Theory*, 135–157. [2](#)

[58] Zhao, J., Chen, L., Pedrycz, W., and Wang, W. (2018). “Variational inference-based automatic relevance determination kernel for embedded feature selection of noisy industrial data.” *IEEE Transactions on Industrial Electronics*, 66(1): 416–428. [2](#)